GA–A23987

HIGH TIME-RESOLVED, 2-D IMAGING OF TYPE-I ELMs IN DIII–D USING A IMAGE-INTENSIFIED CID CAMERA

by
M. GROTH, M.E. FENSTERMACHER, J.A. BOEDO, N.H. BROOKS,
D.S. GRAY, C.J. LASNIER, A.W. LEONARD, G.D. PORTER,
and J.G. WATKINS

JUNE 2002

DISCLAIMER

GA–A23987

HIGH TIME-RESOLVED, 2-D IMAGING OF TYPE-I ELMs IN DIII–D USING A IMAGE-INTENSIFIED CID CAMERA

by
M. GROTH,[†] M.E. FENSTERMACHER,[†] J.A. BOEDO,[‡] N.H. BROOKS, D.S. GRAY,[‡] C.J. LASNIER,[†] A.W. LEONARD, G.D. PORTER,[†] and J.G. WATKINS[◊]

[†]Lawrence Livermore National Laboratory
[‡]University of California, San Diego
[◊]Sandia National Laboratories

This is a preprint of a paper presented at the 15th International Conference on Plasma Surface Interactions in Controlled Fusion Devices, May 27–31, 2002, in Gifu, Japan, and to be published in the *Proceedings.*

Work supported by
the U.S. Department of Energy
under Contracts W-7405-ENG-48, DE-AC03-99ER54463
DE-AC04-94AL85000, and Grant DE-FG03-95ER54294

GA PROJECT 30033
JUNE 2002

ABSTRACT

The evolution of 2-D emission profiles of D_α and C III during type-I ELMs has been investigated in DIII–D using a tangentially viewing gated, intensified charge-injected device (CID) camera. The measured CIII emission profiles indicate transient inner leg attachment with the arrival of the ELM heat pulse. The measured D_α emission profiles during an ELM cycle show enhanced deuterium recycling during the deposition of the ELM particle pulse at the target, which suggests the detachment of the divertor plasma from the target plates. Measurements taken in ELMy H–mode discharges at densities of 50% and 90% of the Greenwald density limit are compared utilising the CID camera system and a comprehensive set of other divertor diagnostics. An ELM model based on fluid and PIC simulations is used to discuss the observation on the response of the divertor plasma to the ELM heat and particle pulse.

1. INTRODUCTION

Large, transient heat fluxes during edge localized modes (ELMs) may cause significant erosion of the divertor target plates in future large tokamaks. Depending on the operational regime, the energy released during an ELM event can be as high as 50% of the pedestal electron energy [1]. The deposition of this energy onto the target plate during a time less than a millisecond can lead to divertor surface ablation and unacceptable target plate erosion [2]. Operational schemes that either avoid large ELMs, or permit the mitigation of their heat fluxes, are under investigation [3]. Some designs propose sharing the ELM heat fluxes in double-null divertor configurations, at the expense of magnetic volume [4,5].

A fast gated, image intensified charge-injected-device (CID) camera, which tangentially views the lower divertor of DIII–D, measures the deuterium (D_α at 656 nm) and carbon (CIII at 465 nm) distribution during the ELM evolution. Using the reconstructed 2-D emission profiles, and taking advantage of the comprehensive, high time-resolving diagnostic system in DIII–D, the response of the divertor plasma to the ELM heat and particle pulse in two operational plasma regimes is characterised.

2. EXPERIMENTAL MEASUREMENT

The measurement of the deuterium and carbon emission profiles augments the existing, sub-millisecond accurate measurements of various plasma parameters in DIII–D (Table 1, Fig. 1). The ELM heat and particle fluxes arriving at the divertor target are measured using infrared thermography [6] and Langmuir probes [7]. Line-integrated measurements of the neutral deuterium emission assess changes in the deuterium recycling [8]. The viewchords cross tangentially at the outboard midplane near the plasma pedestal and scrape-off layer (SOL), and vertically at the core and divertor plasma region.

Table 1. DIII–D Fast diagnostic overview, associated plasma parameters measured, and their time resolution

Diagnostic System	Associated Plasma Parameter	Data Acquisition Rate
Soft X-ray	Electron temperature	10 kHz
Core and divertor Thomson	Electron temperature and density	1 ns @ 140 kHz pulsed (core), 20 Hz (div.)
Interferometer	Line integrated density (divertor outer leg)	50 kHz
Divertor bolometer	Divertor radiated power	10–500 kHz
Midplane and divertor Filterscopes	D_α emission core periphery and divertor	1–100 kHz
Langmuir probes	Target ion saturation current	50 kHz
IRTV	Target heat flux	10 kHz

The installation of a gated, intensified camera has permitted snapshots with a 20 μs integration time to be taken during various times of the ELM evolution for a range of plasma densities [9]. The viewing area of this camera includes the lower divertor region from the floor, –1.36 m, to approximately –0.8 m below the equatorial plane [Fig. 1(b)]. Non-gated, non-intensified CID cameras have been used previously in DIII–D to simultaneously image the deuterium and carbon emission in the visible and ultra-violet wavelength range [10,11].

Two-dimensional profiles of the emission in a poloidal plane are reconstructed from the measured data using a least square minimization technique [12]. Whereas the integration time in a regular CID camera is pre-set to the image acquisition rate of 60 fields/s, in the upgraded camera, a microchannel plate provides the amplifier and fast shutter so that gated exposures as short as 1 μs are obtained within one field, with signal amplification of up to a factor of 10^4. During the course of a discharge, the camera is triggered internally and repetitively, obtaining

snapshots, which are randomly distributed relative to the ELM event. Accurate timing was achieved by digitizing the gate time and dwell as given by the camera control unit. These snapshots are then sorted with respect to the onset of an ELM using the recorded gate times and the time stamp recorded on the video image. Each discharge was repeated to record the emission of D_α and CIII at each density level.

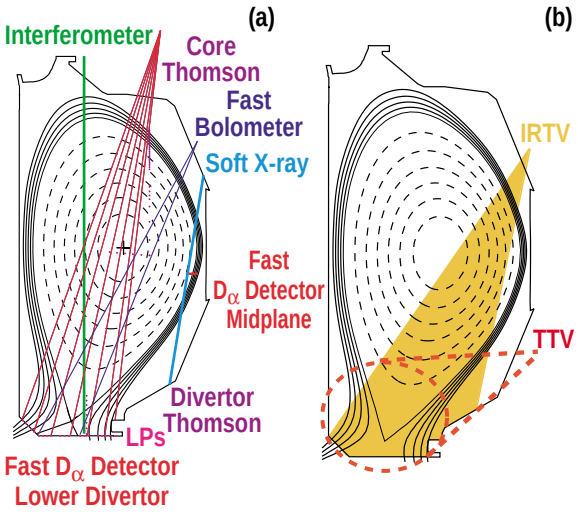

Fig. 1. Viewchords of DIII–D's fast diagnostic systems on magnetic configuration.

Type-I ELMs were studied in neutral beam heated H–mode plasmas run in a lower single-null configuration (Fig. 1). Density control was achieved by simultaneous gas puffing and pumping using the lower cryogenic pump. While maintaining the plasma current (I_p=1.4 MA), toroidal field (B_T=1.8 T), plasma shape (q_{95}=3.5, δ_{up}=0.2), and heating power (P_{NBI}=7 MW) constant, the plasma density was scanned by varying the deuterium gas puff rate from discharge to discharge. H–mode plasmas at 50% of the Greenwald density, n_{GW}, give a normalised energy confinement time of H_{89}=1.8; at higher densities ($0.9n_{GW}$) H_{89}=1.4. The effective plasma ion charge Z_{eff} ranged from 2.5 in low density plasmas to 1.8 at high density. By increasing the plasma density, the ELM frequency increases from 70 Hz to 130 Hz; the ELM amplitude, however, is about three times larger in low density plasmas compared to high density plasmas.

The signature of ELMs in low density plasmas is a rapid rise and a slower recovery at both the inner and outer divertor legs seen by multiple diagnostics. Time histories for some of the fast diagnostics described above are shown in Fig. 2. The distribution of the neutral recycling [Fig. 2(d)] and ion particle fluxes [Fig. 2(e)] at the inner and outer target plate during an ELM was symmetric to within a factor of 2. The particle flux due to an ELM increased as much as two orders of magnitude; the heat flux [Fig. 2(f)] rose as much as three orders of magnitude. The effect of an ELM on the pedestal temperature indicated by a soft x-ray diode [Fig. 2(a)] was a fast drop in the electron temperature, followed by a slow recovery. The midplane recycling [Fig. 2(b)] showed a rapid rise and slow recovery. Given the geometry of the interferometer chord (Fig. 1) it is a good assumption that the electron density perturbation is dominated by the divertor plasma. This measurement [Fig. 2(c)] showed that the density in the outer divertor leg rose rapidly, increasing by 20% during the ELM.

In contrast, high density plasma measurements (not shown) revealed that the ELM heat pulse arrived at the inner target plate only, while the amplitude of the ELM particle pulse was similar

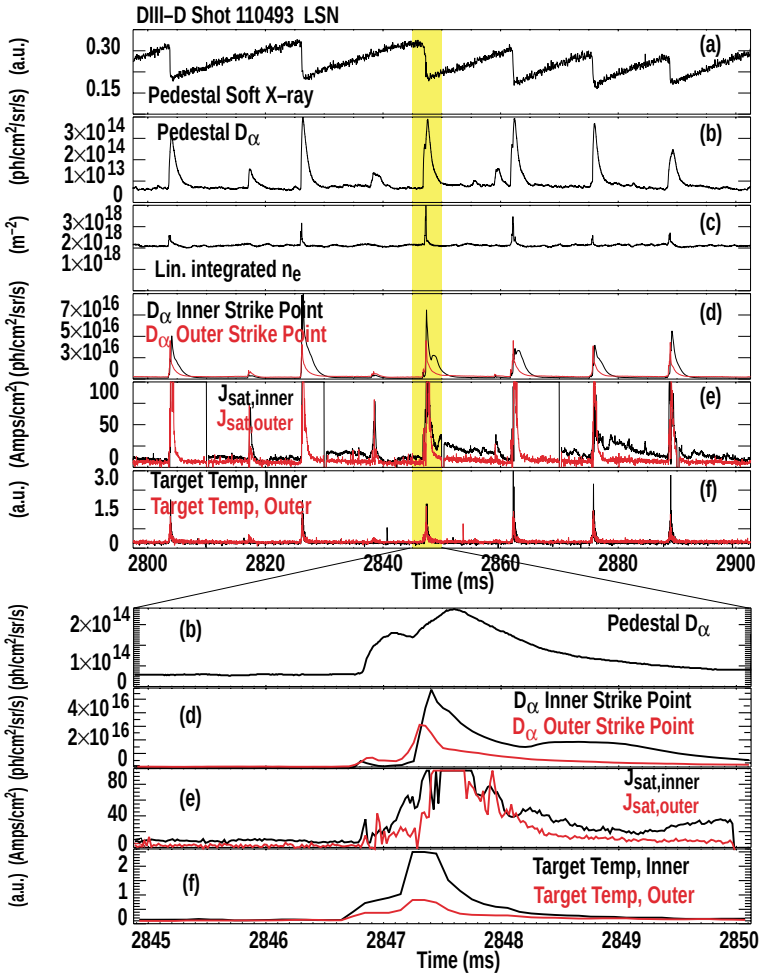

Fig. 2. ELM characteristic of a H–mode plasma at n/n_{GW}~0.5 as observed by the soft x-ray diagnostic (a), the midplane filterscope (b), the vertical interferometer (c), the divertor filterscopes at the inner and outer strike points (d), Langmuir probe ion saturation current at the inner and outer strike point (e), the fast bolometer at the inner and outer strike point (f), and the IRTV peak heat flux at the inner and outer target plate (g).

at both plates. The ELM peak heat flux was reduced to about half of that observed in low density discharges. ELMs perturbed the pedestal temperature only slightly, while there was still a significant pedestal density variation. During an ELM the line-integrated plasma density across the inner divertor leg drops incrementally. While the D_α light at the inner target increases during the ELM burst, at the outer target decreases by more than 50% inner target.

3. EVOLUTION OF 2-D PROFILES DURING AN ELM CYCLE

The CID camera gates once per data acquisition field, so the set of images of the ELM evolution is obtained by collecting snapshots taken at various times during the discharge, and then ordering them with respect to the ELM onset time. Such analysis implicitly assumes that the ELM amplitude and width remain constant throughout the discharge. Postulating that ELMs originate at the outer midplane region of the core pedestal [13], the ELM onset time was determined by applying a numerical ELM finder algorithm to the innermost midplane filterscope signal.

Reconstructed 2-D profiles of the CIII emission (Fig. 3) indicated that in low density ELMy H–mode plasmas a transient attachment of the inner divertor leg occurs at the arrival of the ELM heat pulse. Previous spectroscopy and divertor Thomson measurements have shown that regions of bright CIII emission correspond to electron temperatures of 6–8 eV [9]. Between ELMs the CIII emission in the inner SOL was observed near the X–point [Fig. 3(a) and (3f)], indicating inner leg detachment as observed previously in time-averaged measurements in H–mode plasmas [9]. Approximately 100 μs after the onset of an ELM [Fig. 3(b)] the CIII radiation from the inner divertor region was observed close to the inner target plate, implying re-attachment of the inner leg divertor plasma. In comparison, the timing of the target heat fluxes peaked approximately 400–500 μs after the onset of an ELM at the inner and outer leg. Approximately 600 μs into the ELM cycle the CIII radiation was observed at the X–point again [Fig. 3(e)], but

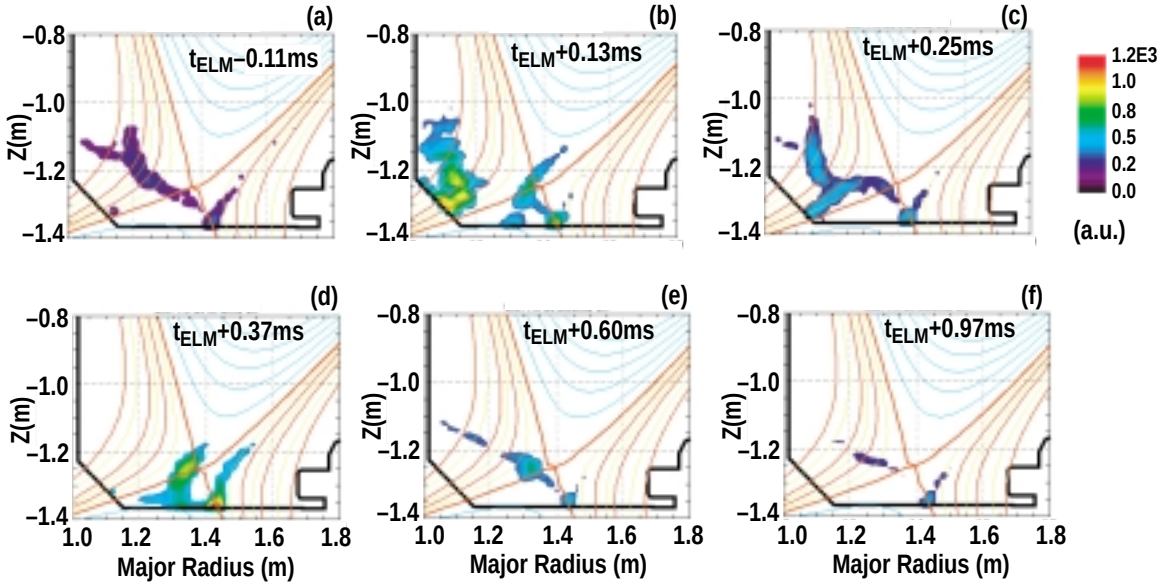

Fig. 3. Evolution of the CIII emission during a type-I ELM, low density H–mode plasma.

at higher intensity. This suggests that the inner divertor leg was detached again. During the ELM evolution, the CIII emission at the outer strike zone changed in magnitude, but remained localized at the target plate. The D_α emission (not shown) was at the inner divertor target and increased by an order of magnitude between 250–400 μs after the ELM onset, but remained close to the target. The plasma returned to its initial state about 1ms after the ELM onset [Fig. 3(f)], thus closing the ELM cycle.

In high density discharges the 2-D emission profiles imply the attachment of the outer divertor leg during the course of an ELM. The CIII emission between ELMs was highly localized at the X–point, which is a signature of a detached divertor plasma. Approximately 250 μs after the ELM onset the CIII radiation was observed at the outer strike point, indicating a transient re-attachment of the divertor outer leg. A corresponding target heat pulse, however, was not observed. After this event, lasting no longer than 300μs, the CIII radiation returned to the X–point. 2-D profiles of the D_α emission showed that the radiation was localized at the inner and outer strike zones with almost no spatial or intensity variation during the ELM cycle.

4. DISCUSSION

Hogan et al. [14], have proposed an ELM model that describes the transient response of an attached divertor plasma to an ELM, which provides some explanation of the experimental observations presented in this paper. According to this model, the divertor plasma temperature initially rises due to the ELM heat pulse, and then decreases dramatically with the dispersal of the ELM ions to the divertor plasma. It is postulated that due to the ion dispersal the electron temperature decreases below the detachment threshold (1–3 eV); a plasma state that lasts 2–3 ms. The initial increase in electron temperature predicted by the model is consistent with the increase of the CIII emission at the outer strike point through increased ion physical sputtering. There is, however, no experimental evidence of transient detachment of the outer divertor plasma. Models that describe the response of a detached plasma to an ELM are desired. It is conceivable that such models will predict the reattachment of the divertor plasma due to the ELM heat pulse.

According to work by Bergmann and Tshakaya using kinetic Particle-In-Cell (PIC) models [15,16], the ELM heat pulse consists of hot electrons, which were expelled from the H–mode pedestal. Accordingly, the estimated transit time of the heat pulse is of the order 3 μs ($T_{e,ped}$~700 eV). In comparison, the transit time of thermal electrons is ~12 μs ($T_{e,SOL}$~35 eV). Unfortunately, such time scales are far too small to be accurately measured by the IRTV.

The duration of the ELM particle dispersal measured by the tangential television is about half the time estimated by Hogan et al. in the low density case, but similar in the high density case. Associating the ELM particle transport with hot ions, the transit time of these ions is approximately 200 μs (cf. 900 μs for thermal ions).

The explanation for the strong in/out asymmetry of the target heat fluxes observed during an ELM in high density plasmas has yet not been found. One hypothesis postulates that the ELM energy is lost due to radiative processes before arriving at the target plate. Measurements of the divertor bolometer array [17] indeed support this thesis; however, the radiated energy accounted for in each ELM is too small to give such significant reduction [18]. 2-D fluid codes, such as UEDGE and B2/EIRENE, should be employed to answer this question.

REFERENCES

[1] A.W. Leonard et al., J. Nucl. Mat. **290-293**, (2001) 1097.

[2] H.D. Pacher, Disruption and ELM Erosion, App. E9, Sec.1.7 (Divertor), ITER Design Description Document, ITER No. G17 DDD 1 96-08-21 W2.1 August 1996

[3] H. Zohm et al., Plasma Physics and Contr. Fusion **38** (1996) 105.

[4] C.J. Lasnier, J. Nucl. Mat **290-293** (2001).

[5] T.W. Petrie et al., "Changes in edge and scrape-off layer plasma behavior due to variation in magnetic balance in DIII–D," these proceedings.

[6] D.N.Hill et al.; Rev. Sci. Instrum. **59** (1988) 1225

[7] J.G. Watkins et al, J. Nucl. Mat. **241-243**, (1997) 645.

[8] R.J. Colchin et al, submitted to Nuclear Fusion (2002).

[9] M.E. Fenstermacher et al., Bulletin of the American Physical Society, **46 (8)** (2001) 225.

[10] M.E. Fenstermacher et al., J. Nucl. Mat.. **241-243** (1997) 666.

[11] M.E Fenstermacher et al., J. Nucl. Mat. **266-269** (1999) 348.

[12] M.E. Fenstermacher et al., Rev. Sci. Instrum. **68** (1997) 974.

[13] P.B. Snyder et al., Phys. Plasmas **9** (2002), 2037.

[14] J.T. Hogan et al., Bulletin of the American Physical Society, **46 (8)** (2001) 223.

[15] A. Bergmann, submitted to Nuclear Fusion (2002).

[16] D. Tshakaya et al. submitted to Plasma Physics and Controlled Fusion (2002).

[17] D.S. Gray et al., Proc. 27th European Conf. on Controlled Fusion and Plasma Physics, Budapest (EPS, 2002) **4**, 121.

[18] A.W. Leonard et al., "Transport of ELM energy and particles into the SOL and divertor of DIII–D," these proceedings.

ACKNOWLEDGMENTS

This work was performed under the auspices of the U.S. Department of Energy under Contracts. DE-AC03-99ER54463 (DIII–D), W-7405-ENG-48 (LLNL), DE-AC04-94AL85000 (SNL) and Grant No. DE-FG03-95ER54294 (UCSD).